Aeroacoustics Conferences
20-23 May 2019, Delft, The Netherlands
25th AIAA/CEAS Aeroacoustics Conference

10.2514/6.2019-2755

Prediction of fine-scale jet mixing noise using geometrical acoustics

Martelet Y.*, Suratteau J.-Y.† and Pont G.‡
Airbus France, Toulouse, France

Bailly C.§
Laboratoire de Mécanique des Fluides et d'Acoustique, UMR CNRS 5509, Ecole Centrale de Lyon, Université de Lyon, 69134 Ecully CEDEX, France

A fine-scale jet mixing noise prediction methodology based on Tam and Auriault model combined with RANS CFD data for the modelling of the sources and geometrical acoustics to account for the propagation is studied. This approach is particularly useful in an industrial context because of its relatively short restitution time. The process is tested on the isolated configurations of the European EXEJET project.

I. Nomenclature

$\hat{}$	=	variable in the Fourier domain
c_{ext}	=	speed of sound in the far field
c_{jet}	=	speed of sound in the jet
G	=	propagation function provided by geometrical acoustics
I	=	amplitude of a source
k	=	wave number
k_t	=	turbulent kinetic energy
k_s	=	kinetic energy related to the fine-scale turbulence
K_D	=	divergence factor
K_T	=	transmission factor
l_s	=	length scale of the fine-scale turbulence
M	=	Mach number
p'	=	pressure fluctuation
p'^a	=	adjoint pressure fluctuation
q_s	=	fine-scale turbulence intensity
r^e	=	radii of curvature of the emerging or reflected wave
S	=	Power spectral density
$\bar{u}_i$	=	mean velocity components
u'_i	=	fluctuating velocity components
ϵ	=	turbulence dissipation
γ	=	specific heat ratio
λ	=	wavelength
ω	=	pulsation
ϕ	=	angle of refraction or reflection
Φ	=	phase jump
ρ	=	local density
$\bar{\rho}$	=	mean density
τ_s	=	decay time

*PhD Student, Acoustic Methods
†Head of Acoustic Methods
‡Engineer, Acoustic Methods
§Professor, AIAA senior member

II. Introduction

Jet mixing noise has been lenghtly studied and comprehensive models have been proposed by Tam and Auriault [1], Morris and Boluriaan [2] and more recently by Miller [3] among others. The request for more accurate predictions and the changes in turbofan-engine geometry have revived the interest in this topic. The jet mixing noise is the noise generated by the turbulent structures located in the mixing layer between the jet and the possible external flow. As described by Tam and Golebiowski [4], the fine-scale and the large-scale turbulence contribute to jet noise. The fine-scale turbulence generates noise which dominates the jet mixing noise spectrum upstream and at a polar angle of 90° whereas the noise associated with the large-scale turbulence dominates the spectrum downstream. The jet mixing noise could be computed using direct acoustic predictions using scale resolving simulations such as direct numerical simulation, large eddy simulation or detached eddy simulation [5] coupled with high accuracy propagators but these solutions are still difficult to apply on complex geometries. A statistical approach is often prefered to calculate aeroacoustic sources using the turbulence data provided by a Reynolds-Averaged Navier-Stokes (RANS) computation. This method is especially useful in an industrial context because of the reasonable restitution time needed for the fluid dynamics computation. Therefore, a design loop can be quickly created in order to evaluate the effect of a geometrical change on the produced noise. The aim of this study is to present a methodology based on Tam and Auriault's model for predicting the jet mixing noise induced by fine-scale turbulence. In addition to the prediction of the refraction through the mixing layer and its associated cone of silence near the jet axis, the methodology aims to also account for the reflection and shielding effects induced by the presence of the pylon and the wing in the propagation field. Ray tracing is used for the propagation in order to correctly take into account all the effects mentioned before. First, the source modelling and the development of the noise spectrum formula following Tam and Auriault's work will be detailed. Then, the problem will be simplified by introducing two homogeneous media and solved using geometrical acoustics. Finally, noise predictions will be shown and compared to a realistic isolated configuration case (EXEJET) [6] at the sideline operating point.

III. Source model for the fine-scale turbulence

Tam and Auriault [1] have developed a method to predict the jet mixing noise using a RANS simulation. The idea is to use the flow data from the simulation in order to compute the source location and amplitude and to propagate the noise from these sources to the far field using a vector adjoint Green function. In the following section their results and the frame of work will be presented. The objective here is to clarify the results that will be used as the stepping stone in the core of this paper and to identify the key steps in their reasoning that will have to be adapted in order to correctly plug the propagation using geometrical acoustics.

Tam and Auriault use a direct approach to solve the problem. The problem can be decomposed in two steps, first the sources then the propagation. Therefore two sets of equation should be taken, first a set of equations governing the propagation of the waves and then another set taking into account the nature and behaviour of the sources. These two sets will then be joined so that the left hand side of the system will act as a wave operator and the right hand side as a source term.

$$\begin{gathered}\bar{\rho}\left[\frac{\partial u_i'}{\partial t}+\bar{u}_j\frac{\partial u_i'}{\partial x_j}+u_j'\frac{\partial \bar{u}_i}{\partial x_j}\right]+\frac{\partial p'}{\partial x_i}=-\frac{\partial q_s}{\partial x_i}\\ \frac{\partial p'}{\partial t}+\bar{u}_j\frac{\partial p'}{\partial x_j}+\gamma\bar{\rho}\frac{\partial u_j'}{\partial x_j}=0\end{gathered} \tag{1}$$

where $\bar{u}_i$ and u_i' are respectively the mean and fluctuating velocity components in Cartesian coordinates, $\bar{\rho}$ is the mean density, p' is the pressure variation and γ is the specific heat ratio.

The source term on the right hand side is

$$q_s=\frac{2}{3}\bar{\rho}k_s \tag{2}$$

with k_s the kinetic energy related to the fine-scale turbulence.

Using adjoint vector Green functions, the pressure is then expressed, refer to [1] in order to get more details in the obtention of the solution. For an appropriate description of the problem, the direction of the axial coordinates coincides with the jet axis. The position of the observer $\vec{x}_M(x_x,x_r,x_\phi)$ and then, the position of two source points $\vec{\xi}_S(\xi_x,\xi_r,\xi_\phi)$ and $\vec{\zeta}_S(\zeta_x,\zeta_r,\zeta_\phi)$ are introduced. The pressure is then expressed as

$$p'(\vec{x}_M,t) = \int_\omega \int_{\vec{\xi}_S} \int_{t_1} \frac{Dq_s}{Dt_1} \hat{p}'^a(\vec{\xi}_S,\vec{x};\omega) e^{-i\omega(t-t_1)} d\omega d\vec{\xi}_S dt_1 \tag{3}$$

$\hat{p}'^a$ is the adjoint pressure in the Fourier domain and $\frac{D}{Dt_1} = \frac{\partial}{\partial t_1} + \bar{u}_x \frac{\partial}{\partial \xi_x}$ is the convective derivative in the axial direction.

By taking the autocorrelation of the pressure, the formula for the noise spectrum is finally obtained. The power spectral density is

$$\hat{S}(\vec{x}_M,\omega) = \int_{\omega_1} \int_{\vec{\xi}_S} \int_{\vec{\zeta}_S} \int_{t_1} \int_{t_2} \hat{p}'^a(\vec{\xi}_S,\vec{x}_M;\omega_1) \hat{p}'^a(\vec{\zeta}_S,\vec{x}_M;\omega) \left\langle \frac{Dq_s(\vec{\xi}_S,t_1)}{Dt_1} \frac{Dq_s(\vec{\zeta}_S,t_2)}{Dt_2} \right\rangle e^{-i(\omega_1+\omega)t+i\omega_1 t_1+i\omega t_2} d\omega_1 d\vec{\xi}_S d\vec{\zeta}_S dt_1 dt_2 \tag{4}$$

where S_s is defined as

$$S_s = \left\langle \frac{Dq_s(\vec{\xi}_S,t_1)}{Dt_1} \frac{Dq_s(\vec{\zeta}_S,t_2)}{Dt_2} \right\rangle \tag{5}$$

The autocorrelation of the sources S_s must now be modelled. The correlation function for the full convective derivative has not yet been measured but Davies et al. [7] studied and measured the two-point space-time correlation of the fluctuating axial velocity component in jets. Tam and Auriault argued that the autocorrelation function they need should be similar to the one from Davies et al. The model function used for the autocorrelation is the following.

$$\left\langle \frac{Dq_s(\vec{\xi}_S,t_1)}{Dt_1} \frac{Dq_s(\vec{\zeta}_S,t_2)}{Dt_2} \right\rangle = \frac{\hat{q}_s^2}{c^2\tau_s^2} \exp\left(-\frac{|\xi_x - \zeta_x|}{\bar{u}_x \tau_s} - \ln 2 \left[\frac{[(\xi_x - \zeta_x) - \bar{u}_x(t_1 - t_2)]^2}{l_s^2} + \frac{(\xi_y - \zeta_y)^2}{l_s^2} + \frac{(\xi_z - \zeta_z)^2}{l_s^2} \right] \right) \tag{6}$$

and when $\vec{\xi}_S \to \vec{\zeta}_S$ and $t_1 \to t_2$

$$\left\langle \left(\frac{Dq_s(\vec{x},t)}{Dt} \right)^2 \right\rangle = \frac{\tilde{q}_s^2}{c^2\tau_s^2} = \frac{I_s^2}{\tau_s^2} \tag{7}$$

In this expression, a few key terms need to be defined

$$\begin{aligned} \frac{\tilde{q}_s}{c} &= Aq = A\frac{2}{3}\bar{\rho}k_t = I_s \\ l_s &= c_l \frac{k_t^{3/2}}{\epsilon} \\ \tau_s &= c_\tau \frac{k_t}{\epsilon} \end{aligned} \tag{8}$$

Here, k_t is the turbulent kinetic energy, ϵ is the turbulence dissipation and c is the local sound celerity. l_s is the length scale of the fine-scale turbulence and τ_s is the decay time. $\tilde{q}_s$ is a measure of the intensity of the temporal fluctuation of the kinetic energy of the fine-scale tubulence. The adjustment constants are set by Tam and Auriault [1] to be $A = 1.5855$, $c_l = 0.256$ and $c_\tau = 0.233$. Having RANS CFD computations, all these terms can be computed and thus the whole source term. It might seem surprising that even though it was explained earlier with the definition of q_s in Eq. (2) that the turbulent kinetic energy k_s (and thus the turbulent dissipation ϵ) used was only the one responsible for fine-scale turbulence, the value used for the modelling of the sources in Eq. (8) is directly the one given by the RANS simulation and does not take any kind of filtering on the size of the turbulent structure. Tam and Auriault argue that k_s and k_t should be proportional, hence the introduction of the adjustment constants.

The autocorrelation function presented above can be assimilated as a Gaussian function in four dimensions. It can be separated in two parts, first the height of the curve's peak expressed in Eq. (7) then the attenuation factor being the exponent. What is expressed here is that the correlation of two source points at two given time is a function of the difference in distance between these two points and the difference between the two time-steps.

A smaller spatial difference leads to a higher correlation with a maximum being expressed in Eq. (7) and on the contrary a higher spatial difference will drive the correlation function to zero. The rate at which the correlation function will decrease is controled by the choice of the length scales l_s as in any Gaussian function. Here these length scales are the one from the fine-scale turbulence, meaning that only sources within a single structure will be coherent. That describes the physics well because as explained in [8], the fine-scale turbulence jet mixing noise is a compact source. Note that the use of Gaussian functions to describe the evolution of the coherence depending on the distance between the source points is justified empirically with measurements presented in [7]. The same analysis can be done concerning the correlation in time while noting the difference in rate of the decrease with the time difference. This is also motivated by the results of experiments presented in [7] showing that the effect on the correlation could be assimilated to an exponential decrease and not a Gaussian function. Morris and Boluriaan [2] and Miller [3] introduced similar formulations of the time-space correlation function using slightly clearer formulations. Despite the difference in the formulation, the modelling of the autocorrelation of the sources remains Gaussian fit.

As for the amplitude of this correlation function, one could see it as a scaling of the kinetic energy over a time scale which here would be the life expectancy of the turbulent structure or, as describe by Tam, the decay time. Although q_s is evaluated at two separated position and time in the left hand side of Eq. (6), $\tilde{q}_s$, τ_s and l_s are evaluated at an unspecified position and time in the right hand side. Using the compactness of the sources, if two source points are close enough that their correlation is not null, the value of both the decay time and the kinetic energy should be very close. That would justify evaluating I_s and l_s in either $(\vec{\xi}_S, t_1)$ or $(\vec{\zeta}_S, t_2)$.

Substituting Eq. (6) in Eq. (4) gives

$$S(\vec{x}_M,\omega) = \int_{\omega_1}\int_{\vec{\xi}_S}\int_{\vec{\zeta}_S}\int_{t_1}\int_{t_2} \frac{I_s^2}{\tau_s^2}\exp\left(-\frac{|\xi_x-\zeta_x|}{\bar{u}_x\tau_s} - \ln 2\left[\frac{[(\xi_x-\zeta_x)-\bar{u}_x(t_1-t_2)]^2}{l_s^2} + \frac{(\xi_y-\zeta_y)^2}{l_s^2} + \frac{(\xi_z-\zeta_z)^2}{l_s^2}\right]\right) \hat{p}'^a(\vec{\xi}_S,\vec{x}_M;\omega_1)\hat{p}'^a(\vec{\zeta}_S,\vec{x}_M;\omega)e^{-i(\omega_1+\omega)t+i\omega_1 t_1+i\omega t_2}d\omega_1 d\vec{\xi}_S d\vec{\zeta}_S dt_1 dt_2 \tag{9}$$

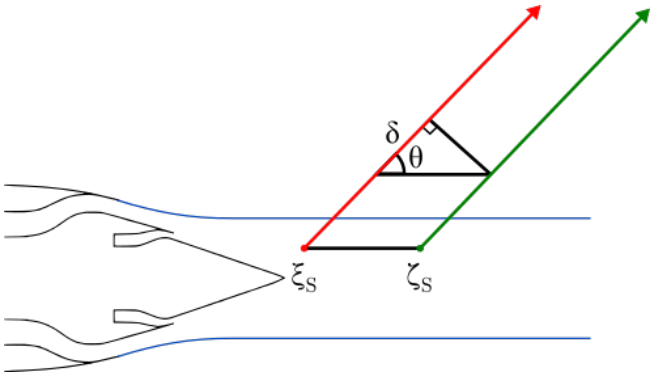

Fig. 1 Illustration of the difference in ray paths between two source points ξ and ζ from a far-field point x

The next step is to work on the propagation part so that the double integration over the source domain is reduced to a single integration thus making the calculation way lighter. Considering an observer at the far field, Tam and Auriault write that the propagation from a source point ξ_S and the observer and one between a source point ζ_S and the observer are straight and parallel and only differ in length by $\delta = (\xi_x - \zeta_x)\cos\theta$, with θ the polar angle of the observer in the spherical coordinates. This is pictured in Fig. 1. That means that their propagation only differ by a phase jump. From this comes the following relation between the adjoint pressure fluctuation for two source points nearby

$$\hat{p}'^a(\vec{\xi}_S,\vec{x}_M;-\omega) = \hat{p}'^a(\vec{\zeta}_S,\vec{x}_M;-\omega)\exp\left[i\frac{\omega}{c_{ext}}\cos\theta(\xi_x-\zeta_x)\right] \tag{10}$$

with c_{ext} the speed of sound at the far field.

It should be noted that this approximation only holds for two source points located very close from each other which is not always the case. Nevertheless the expression of the autocorrelation of the sources in Eq. (6) has the advantage of

being null in the case of two source points far from each other. Therefore, the approximation can be written on all the source domain.

The integrations over the source domain can now be performed and the reader should here again refer to Tam and Auriault [1]. The final expression for the radiated sound is

$$S(\vec{x}_M,\omega) = 4\pi\left(\frac{\pi}{\ln 2}\right)^{3/2}\int_{\vec{\zeta}_S}\frac{I_s^2 l_s^3}{\tau_s}|\hat{p}'^a(\vec{\zeta}_S,\vec{x}_M;\omega)|^2\frac{\exp\left[-\dfrac{\omega^2 l_s^2}{4\ln 2\bar{u}_x^2}\right]}{1+\left(1-\dfrac{\bar{u}_x}{c_{ext}}\cos\theta\right)^2\omega^2\tau_s^2}d\vec{\zeta}_S \tag{11}$$

This expression of S is not directly usable. An expression of the adjoint pressure needs to be found in order to obtain the noise spectra. The following section will present a way to predict the radiated sound using geometrical acoustics.

IV. Fine-scale jet mixing noise prediction in two associated homogeneous media

Tam and Auriault provided a near-complete method for fine-scale jet mixing noise prediction.However, $\hat{p}'^a$ needs to be found in order to properly obtain the noise spectra. The numerical resolution of the adjoint LEE could be done, but this approach unfortunately does not fit in the industrial requirements set in the introduction. The idea is therefore to keep the general structure of the development of the method presented in the previous section but to simplify the physics in order to make it easier to compute the propagation part. In a first part, a new set of equation will be introduced in order to get a problem easier to solve and requiring less computation time. Then the calculations will be carried on to obtain a usable formula for the noise spectrum.

A. Formulation of the problem in an association of two homogeneous media

First, let's consider a first medium labelled "jet". It will be considered that the jet plume is a homogeneous medium with uniform mean flow. Tam and Auriault used Eq. (1) as a starting point to describe the physics and the same will be done here for the medium jet following the works from Brouwer and Nijboer [9].

The linearised Euler equations are

$$\begin{aligned}\bar{\rho}\left[\frac{\partial u_i'}{\partial t}+\bar{u}_j\frac{\partial u_i'}{\partial x_j}+u_j'\frac{\partial \bar{u}_i}{\partial x_j}\right]+\frac{\partial p'}{\partial x_i} &= -\frac{\partial q_s}{\partial x_i}\\ \frac{\partial p'}{\partial t}+\bar{u}_j\frac{\partial p'}{\partial x_j}+\gamma\bar{p}\frac{\partial u_j'}{\partial x_j} &= 0\end{aligned} \tag{12}$$

with a uniform and parallel mean flow that reduces to

$$\begin{aligned}\bar{\rho}\frac{Du'}{Dt}+\frac{\partial p'}{\partial x_i} &= -\frac{\partial q_s}{\partial x_i}\\ \frac{Dp'}{Dt}+\gamma\bar{p}\frac{\partial u_j'}{\partial x_j} &= 0\end{aligned} \tag{13}$$

with the convective derivative defined as

$$\frac{D}{Dt} = \frac{\partial}{\partial t}+\bar{u}_j\frac{\partial}{\partial x_j} = \frac{\partial}{\partial t}+\bar{u}\cdot\nabla \tag{14}$$

Taking the divergence of the momentum equation and the convective derivative of the continuity equation leads to

$$\bar{\rho}\frac{D}{Dt}\nabla u' + \nabla^2 p' = -\nabla^2 q_s \tag{15}$$

$$\frac{D^2 p'}{Dt^2}+\bar{\rho}c_{jet}^2\frac{D}{Dt}\nabla u' = 0 \tag{16}$$

with $c_{jet} = \sqrt{\gamma \frac{\bar{p}}{\bar{\rho}}}$

Subtracting Eq. (16) and Eq. (15) allows to derive the following wave equation

$$\frac{1}{c_{jet}^2}\frac{D^2 p'}{Dt^2} - \nabla^2 p' = \nabla^2 q_s \tag{17}$$

known as the convected Helmholtz equation.

Now let's introduce a second medium labelled "ext" around the jet with the same properties but containing no source. It corresponds to the external flow. A similar development can be done giving another convected Helmholtz equation. It should be noted that some obstacles can be present in this medium such as a wing or a pylon. This way, Eq. (18) can also be used in the case of an installed jet.

$$\frac{1}{c_{ext}^2}\frac{D^2 p'}{Dt^2} - \nabla^2 p' = 0 \tag{18}$$

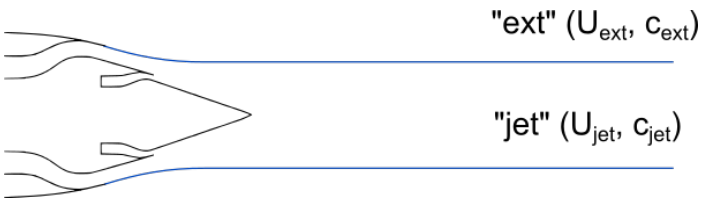

Fig. 2 Illustration of the two homogeneous media

The association of the two media is pictured in Fig. 2. In this configuration, described by the junction of these two convected Helmholtz equations is the sound propagation in two associated homogeneous media with sources of amplitude $\nabla^2 q_s$. The resolution of this problem can be done using geometrical acoustics. Indeed, if the wavelength is greatly inferior to the characteristic length of the problem, here the radius of the nozzle, the plane-wave approximation can be taken. That means that if $R_{jet} \gg \lambda$ the pressure at the far field can be expressed as

$$p'(\vec{x}_M, t) = \int_\omega \int_{\vec{\xi}_S} \int_{t_1} \hat{G}(\vec{x}_M, \vec{\xi}_S, \omega) e^{-i\omega(t-t_1)} \nabla^2 q_s(\vec{\xi}_S, t_1) d\omega d\vec{\xi}_S dt_1 \tag{19}$$

with $\hat{G}$ the transfer function given by geometrical acoustics in the Fourier domain [10].

This high frequency approximation allows the asymptotic approach of the Green function to account for the refraction and reflections effects. It will be here chosen to neglect the diffraction. This high frequency approximation also suggests that the diffraction can be neglected on the considered frequency range. The classical criteria for the application of the geometrical is $R_{jet} \gg \lambda$. Nevertheless, years of work with such techniques at Airbus have shown that even if it seems surprising for the lower part of the frequency range, the results using ray techniques still holds as low as $kR_{jet} > 2$.

Now that the propagation part has been presented, its compatibility with the source model has to be justified. The following calculations will show how an analog formula as Eq. (11) can be obtained. The first objective is to obtain an expression similar to Eq. (3) in order to introduce the source model as given by Tam and Auriault. Indeed, the following term needs to appear

$$\left\langle \frac{Dq_s(\vec{\xi}_S, t_1)}{Dt_1} \frac{Dq_s(\vec{\zeta}_S, t_2)}{Dt_2} \right\rangle \tag{20}$$

Applying an integration by parts twice gives

$$p'(\vec{x}_M, t) = \int_\omega \int_{\vec{\xi}_S} \int_{t_1} \nabla^2 \hat{G}(\vec{x}_M, \vec{\xi}_S, \omega) e^{-i\omega(t-t_1)} q_s(\vec{\xi}_S, t_1) d\omega d\vec{\xi}_S dt_1 \tag{21}$$

because $q_s = 0$ outside of the jet. Note that the divergence is done on $\vec{\xi}_S$, the coordinate of the sources. In the case where $\vec{\xi}_S \neq \vec{x}_M$, there is the following relation

$$\frac{1}{c_{jet}^2}\hat{D}^2\hat{G} = \nabla^2\hat{G} \tag{22}$$

with the convective derivative in the Fourier domain

$$\hat{D} = -i\omega + \bar{u}_{jet}\cdot\nabla \tag{23}$$

and in the time domain

$$\frac{D}{Dt} = \frac{\partial}{\partial t} + \bar{u}_{jet}\cdot\nabla \tag{24}$$

Inserting (22) in Eq. (21) gives

$$p'(\vec{x}_M,t) = \frac{1}{c_{jet}^2}\int_\omega\int_{\vec{\xi}_S}\int_{t_1}\hat{D}^2\hat{G}(\vec{x}_M,\vec{\xi}_S,\omega)e^{-i\omega(t-t_1)}q_s(\vec{\xi}_S,t_1)d\omega d\vec{\xi}_S dt_1 \tag{25}$$

An integration by part gives

$$p'(\vec{x}_M,t) = \frac{1}{c_{jet}^2}\int_{\vec{\xi}_S}\int_{t_1}\hat{D}\hat{G}(\vec{x}_M,\vec{\xi}_S,\omega)e^{-i\omega(t-t_1)}\frac{Dq_s}{Dt}(\vec{\xi}_S,t_1)d\vec{\xi}_S dt_1 \tag{26}$$

This equation can be put directly in parallel with Eq. (3) with

$$\hat{p}'_a(\vec{\xi}_S,\vec{x}_M,\omega) \sim \frac{1}{c_{jet}^2}\hat{D}\hat{G}(\vec{x}_M,\vec{\xi}_S,\omega) \tag{27}$$

In our asymptotic approach, there can be multiple rays coming from $\vec{\xi}_S$ and reaching $\vec{x}_M$, $\hat{G}$ can be written as a sum of the contributions of the different rays such as

$$\hat{G}(\vec{x}_M,\vec{\xi}_S,\omega) = \sum_{r=1}^{N(\vec{\xi}_S)}\hat{G}_r(\vec{x}_M,\vec{\xi}_S,\omega) \tag{28}$$

That gives

$$p'(\vec{x}_M,t) = \frac{1}{c_{jet}^2}\int_\omega\int_{\vec{\xi}_S}\int_{t_1}\frac{Dq_s}{Dt_1}\left[\hat{D}\sum_{r=1}^{N(\vec{\xi}_S)}\hat{G}_r(\vec{x}_M,\vec{\xi}_S,\omega)\right]e^{-i\omega(t-t_1)}d\omega d\vec{\xi}_S dt_1 \tag{29}$$

Calculations analog to the one used to go from Eq. (3) to Eq. (4) are done, giving

$$\hat{S}(\vec{x}_M,\omega) = \frac{1}{c_{jet}^4}\int_{\omega_1}\int_{\vec{\xi}_S}\int_{\vec{\zeta}_S}\int_{t_1}\int_{t_2}\left[\hat{D}\sum_{r=1}^{N(\vec{\xi}_S)}\hat{G}_r(\vec{x}_M,\vec{\xi}_S,\omega_1)\right]\left[\hat{D}\sum_{r=1}^{N(\vec{\zeta}_S)}\hat{G}_r(\vec{x}_M,\vec{\zeta}_S,\omega)\right]\left\langle\frac{Dq_s(\vec{\xi}_S,t_1)}{Dt_1}\frac{Dq_s(\vec{\zeta}_S,t_2)}{Dt_2}\right\rangle$$
$$e^{-i(\omega_1+\omega)t+i\omega_1 t_1+i\omega t_2}d\omega_1 d\vec{\xi}_S d\vec{\zeta}_S dt_1 dt_2 \tag{30}$$

The source model can now be introduced. In their paper, Tam and Auriault identical length scales using $l_x = l_y = l_z = l_s$. This view is not shared by all the scientific community. As an example, Fleury et al [11] measured a factor two between the transverse and axial length scales in the case of the isotropic turbulence. Therefore, this expression of the autocorrelation function will be used instead

$$\left\langle\frac{Dq_s(\vec{\xi}_S,t_1)}{Dt_1}\frac{Dq_s(\vec{\zeta}_S,t_2)}{Dt_2}\right\rangle = \frac{I_s^2}{\tau_s^2}\exp\left(-\frac{|\xi_x-\zeta_x|}{\bar{u}_x\tau_s} - \ln 2\left[\frac{[(\xi_x-\zeta_x)-\bar{u}_x(t_1-t_2)]^2}{l_x^2} + \frac{(\xi_y-\zeta_y)^2}{l_y^2} + \frac{(\xi_z-\zeta_z)^2}{l_z^2}\right]\right) \tag{31}$$

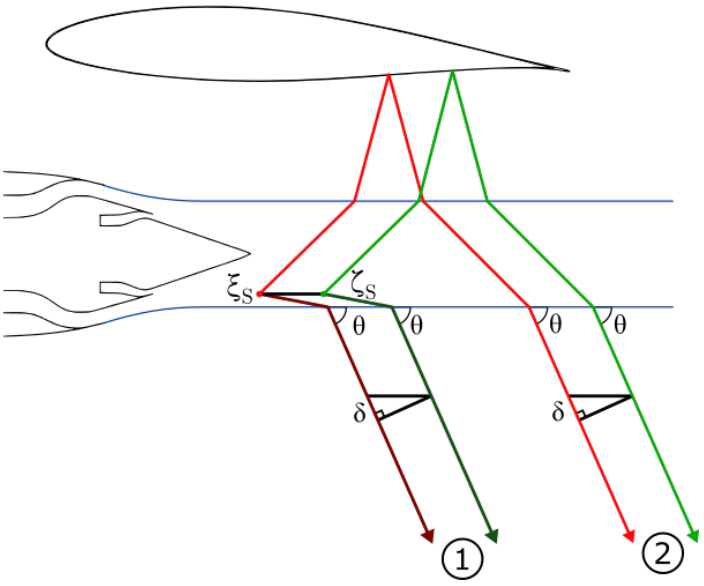

Fig. 3 Illustration of the difference in multiple ray paths between two source points ξ_S and ζ_S perceived by a far-field observer x_M in the case of an installed configuration

It is not yet possible to jump forward to something analog to Eq. (11) with the updated propagation term because the far field and compactness approximation is not straightforward. In this case there are several key differences, one being that the rays are not straight anymore like in Fig. 1 but can be very complex if there are several reflections or refractions but there might also be several rays from one single source that could reach the observer. Such a complex case is pictured in Fig.3. In this case, it is fair to consider that for two sources close enough to each other all the rays reaching x_M can be paired. See the pairs between the light rays, associated with the subscript 1 and the dark rays, associated with the subscript 2. For each pair, the paths are of equal lengths up until the last segment. Given that the observer is at the far field, last segments of the rays reaching it can be considered parallel and they make the same polar angle of θ with the jet axis. Therefore the difference in path for each pair will be δ just like in Fig. 1.

In Morris and Boluriaan [2], a more general, 3D version of Eq. (10) is proposed

$$\hat{p'}^a(\vec{\xi}_S,\vec{x}_M;-\omega) = \hat{p'}^a(\vec{\zeta}_S,\vec{x}_M;-\omega)\exp\left(i\frac{\omega}{c_{ext}\parallel\vec{x}_M\parallel}\vec{x}_M\cdot(\vec{\xi}_S-\vec{\zeta}_S)\right) \tag{32}$$

This will be used here, giving

$$\hat{G}_1(\vec{x}_M,\vec{\xi}_S,-\omega) = \hat{G}_1(\vec{x}_M,\vec{\zeta}_S,-\omega)\exp\left[i\frac{\omega}{c_{ext}}\Big(\cos\theta(\xi_x-\zeta_x)+\sin\theta\cos\phi(\xi_y-\zeta_y)+\sin\theta\sin\phi(\xi_z-\zeta_z)\Big)\right] \tag{33}$$

$$\hat{G}_2(\vec{x}_M,\vec{\xi}_S,-\omega) = \hat{G}_2(\vec{x}_M,\vec{\zeta}_S,-\omega)\exp\left[i\frac{\omega}{c_{ext}}\Big(\cos\theta(\xi_x-\zeta_x)+\sin\theta\cos\phi(\xi_y-\zeta_y)+\sin\theta\sin\phi(\xi_z-\zeta_z)\Big)\right] \tag{34}$$

$$\hat{G}_1(\vec{x}_M,\vec{\xi}_S,-\omega)+\hat{G}_2(\vec{x}_M,\vec{\xi}_S,-\omega) = \Big(\hat{G}_1(\vec{x}_M,\vec{\zeta}_S,-\omega)+\hat{G}_2(\vec{x}_M,\vec{\zeta}_S,-\omega)\Big)\exp\left[i\frac{\omega}{c_{ext}}\Big(\cos\theta(\xi_x-\zeta_x)+\sin\theta\cos\phi(\xi_y-\zeta_y)+\sin\theta\sin\phi(\xi_z-\zeta_z)\Big)\right] \tag{35}$$

Thus, in the general case there is

$$\sum_{r=1}^{N(\vec{\xi}_S)} \hat{G}_r(\vec{x}_M,\vec{\xi}_S,-\omega) = \left(\sum_{r=1}^{N(\vec{\zeta}_S)} \hat{G}_r(\vec{x}_M,\vec{\zeta}_S,-\omega)\right) \exp\left[i\frac{\omega}{c_{ext}}\Big(\cos\theta(\xi_x-\zeta_x)+\sin\theta\cos\phi(\xi_y-\zeta_y)+\sin\theta\sin\phi(\xi_z-\zeta_z)\Big)\right] \tag{36}$$

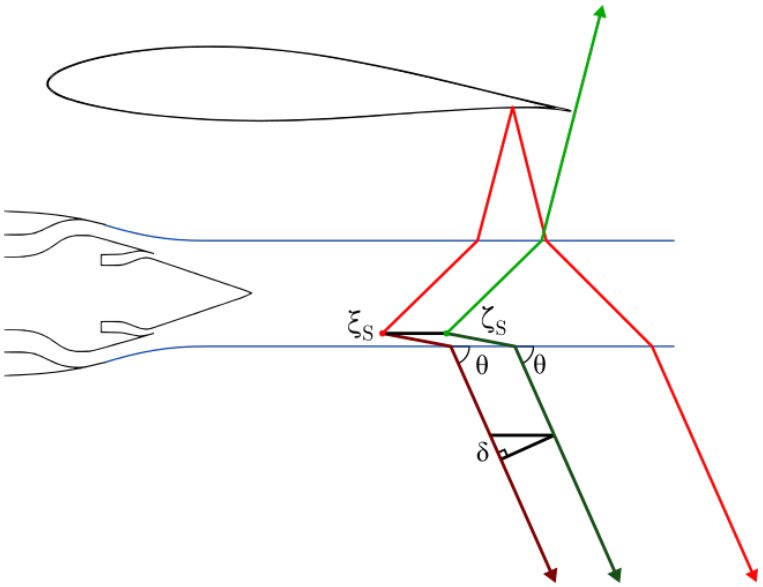

Fig. 4 Illustration of an extreme case where two sources close to each other do not have matching rays

In some extreme cases the rays coming from two sources close to each other cannot be paired. An example is pictured in Fig. 4 with the case of one ray reflecting just before the tip of the wing and one ray missing the wing. It will be chosen to neglect these cases considering the rarity of the event and the size of the correlation scales.

It has been proven that the far field and compactness approximation done by Tam and Auriault can be extended in the case of sources sending multiple rays and in cases as complex as installed configurations.

Using the fact that

$$\sum_{r=1}^{N(\vec{\zeta}_S)} \hat{G}_r(\vec{x}_M,\vec{\zeta}_S,-\omega) = \sum_{r=1}^{N(\vec{\zeta}_S)} \hat{G}_r^*(\vec{x}_M,\vec{\zeta}_S,\omega) \tag{37}$$

that leads to

$$\hat{S}(\vec{x}_M,\omega) = 2\pi\left(\frac{\pi}{\ln 2}\right)^{1/2}\int_{\vec{\xi}_S}\int_{\vec{\zeta}_S}\frac{I_s^2 l_x}{\tau_s^2\bar{u}_x c_{jet}^4}\left|\hat{D}\sum_{r=1}^{N(\vec{\zeta}_S)}\hat{G}_r(\vec{x}_M,\vec{\zeta}_S,\omega)\right|^2 \exp\left[i\frac{\omega}{c_{ext}}\Big(\cos\theta(\xi_x-\zeta_x)+\sin\theta\cos\phi(\xi_y-\zeta_y)+\sin\theta\sin\phi(\xi_z-\zeta_z)\Big)\right] \exp\left[-\frac{\omega^2 l_x^2}{(4\ln 2)\bar{u}_x^2}-\frac{|\xi_x-\zeta_x|}{\bar{u}_x\tau_s}\right]\exp\left[-\ln 2\left[\frac{(\xi_y-\zeta_y)^2}{l_y^2}+\frac{(\xi_z-\zeta_z)^2}{l_z^2}\right]-\frac{i\omega(\xi_x-\zeta_x)}{\bar{u}_x}\right]d\vec{\xi}_S d\vec{\zeta}_S \tag{38}$$

It is straightforward to deduce the final radiated noise formula by following Tam and Auriault. That gives

$$\hat{S}(\vec{x}_M,\omega) = 4\pi\left(\frac{\pi}{\ln 2}\right)^{3/2}\iiint_{-\infty}^{\infty}\frac{I_s^2 l_x l_y l_z}{\tau_s c_{jet}^4}\left|\hat{D}\sum_{r=1}^{N(\vec{\zeta}_S)}\hat{G}_r(\vec{x}_M,\vec{\zeta}_S,\omega)\right|^2 \frac{\exp\left[-\frac{\omega^2}{4\ln 2\bar{u}_x^2}\left(l_x^2+\frac{\bar{u}_x^2}{c_{ext}^2}[l_y^2\sin^2\theta\cos^2\phi + l_z^2\sin^2\theta\sin^2\phi]\right)\right]}{1+\left(1-\frac{\bar{u}_x}{c_{ext}}\cos\theta\right)^2\omega^2\tau_s^2} d\vec{\zeta}_S \tag{39}$$

For clarity reason, the previous expression will be written in a simpler way as

$$\hat{S}(\vec{x}_M,\omega) = \iiint_{-\infty}^{\infty}\left|\Pi(\vec{x}_M,\vec{\zeta}_S,\omega)\right|^2 A_s(\vec{x}_M,\vec{\zeta}_S,\omega)d\vec{\zeta}_S \tag{40}$$

with

$$\Pi(\vec{x}_M,\vec{\zeta}_S,\omega) = \hat{D}\sum_{r=1}^{N(\vec{\zeta}_S)}\hat{G}_r(\vec{x}_M,\vec{\zeta}_S,\omega) = \hat{D}\hat{G}(\vec{x}_M,\vec{\zeta}_S,\omega) \tag{41}$$

$$A_s(\vec{x}_M,\vec{\zeta}_S,\omega) = 4\pi\left(\frac{\pi}{\ln 2}\right)^{3/2}\frac{I_s^2 l_x l_y l_z}{\tau_s c_{jet}^4}\frac{\exp\left[-\frac{\omega^2}{4\ln 2\bar{u}_x^2}\left(l_x^2+\frac{\bar{u}_x^2}{c_{ext}^2}[l_y^2\sin^2\theta\cos^2\phi + l_z^2\sin^2\theta\sin^2\phi]\right)\right]}{1+\left(1-\frac{\bar{u}_x}{c_{ext}}\cos\theta\right)^2\omega^2\tau_s^2} \tag{42}$$

The first term, Π, will be named propagation term because it contains the information of all the different rays. This will be computed using an in-house ray tracing tool. The second term, A_s will be referred as the source term even though it contains a remnant of the far field and compactness approximation that is technically linked with the propagation. This term will be computed using a RANS computation. In the end, both terms will be assembled and summed for all sources.

V. Application

Jet mixing noise prediction will be presented and compared to the EXEJET test case. In this configuration, the diameter of the core and the bypass are respectively 130mm and 220mm. The measurements and the prediction are both made for an isolated configuration at sideline condition with an external flow. That means $M_{jet} = 0.78$ and M_{ext}=0.23. This operating point provides realistic flow conditions, a validated jet noise signal and a sizeable flight effect. As a side note, the jet is coaxial even though this is not taken into account in the model and with a temperature ratio $T_{core}/T_{fan} = 2.43$.

As presented in the previous section, the propagation is handled using two associated homogeneous media. If it is easily admitted that the external medium is homogeneous, it is not that obvious for the jet plume. It is necessary to define this last medium with first its geometry then its characteristics. Using a filtering method, based on the vorticity and the turbulent viscosity fields, the jet plume is delimited. In a second time, a CAD surface is built to contain this medium. Considering that the jet is a homogeneous medium is a very strong approximation, especially when using a double flow nozzle. Even though it could be more finely tuned, the Mach chosen for this part of the propagation is $M_{jet} = 0.78$. It could be interesting to evaluate the impact of this value in terms of predicted noise level but one could expect the apparition of the cone of silence more downstream when using a lower Mach number for the jet. In these conditions the theoretical angle for the cone of silence is around 125°.

In this sections three sets of spectra will be compared.

- Noise predictions using the source model as presented by Tam and Auriault and a propagation in two associated homogeneous media as presented in the previous section. This will be labelled as "T&A + Rays" in the plots.

- Noise predictions using the source model as presented by Tam and Auriault and a uniform propagation medium, the external flow and therefore the convected Helmholtz equation as the wave operator instead of Eq. (41). This will be labelled as "T&A + CHE" in the plots.
- Measurements from wind tunnel experiments. This will be labelled as "Measurements" in the plots

Both predicted methods will use the same source model A_s from Eq. (42). This term is computed using RANS computations. Regarding the propagation using geometrical acoustics, an in-house ray tracing tool will be used to obtain Π from Eq. (41). In this last term, only the first generation of transmitted rays will be taken into account. That means that rays reflecting inside the jet plume before exiting it and reaching the observer will be neglected.

The comparison of the three sets of spectra are shown in Fig. 5. Both noise predictions give results that are close in both shape and level. This is due to the fact that the source model is identical for both models. The predictions are relatively good, especially when looking at the peak amplitude. The predictions are better when using geometrical acoustics with a good agreement up until 120°. The amplitude of the peak increases gradually, matching the value obtained with the experiments. Above this polar angle, the noise level drops dramatically with the apparition of the cone of silence. Because the propagation medium in the jet plume has a lower refraction index than the external medium, there is a limit value for the refracted angle creating a zone downstream where no rays can be propagated. That effects cannot be seen in the predictions using the convected Helmholtz equation since no refraction is computed. The presence of this physical effect in the results confirms the quality of the code and the added value of geometrical acoustics. It might be surprising that even though it was stated that the cone of silence is a physical phenomenon, it cannot be observed in the experiments. That is justified by the fact that downstream, the large-scale turbulence drives the spectrum as explained by Tam et al [4]. This second spectrum driving the total jet mixing noise can also be seen by looking at the shape of the spectrum from the measurements. One can guess the progressive emergence of a secondary, narrower spectrum. It is especially visible at 135° and 150°. This noise source is not predicted by the present model, therefore the spectra cannot be compared downstream. When focusing on the directivity by comparing the OASPL in Fig 6 for all three sets of spectra, the cone of silence is even more visible. In terms of OASPL, the predictions using the two homogeneous propagation media leads to better results. The position of the cone of silence agrees well with the theoretical value of 125° given above. Yet, the shape of the PSD spectra does not completely agree with the measurements when looking at the slope at high frequencies. The peak of the spectra from the experiments are narrower. It can also be noted that the peak frequency is also slightly overestimated, mainly upstream. A tuning of the constants in Eq. (8) would lead to an improvement on these topics, nevertheless considering the nozzle used, it might be too early in the development of the prediction model to perform this tuning.

However, a damper has to be put on the results. As mentionned above geometrical acoustics is an approximation that does not hold on the whole frequency range. When the wavelength cannot be considered small compared to the curvature of the surface on which the wave will be refracted. With this test case, acceptable results could be expected above 300Hz. That would still keep the results in the range around the peak in the zone of validity which is the frequency main band of interest. In terms of performance, the aim was to keep the computation time quite low in order to use this method in design loops. The production a spectrum of an isolated jet if the RANS computation is provided can be done under an hour which is within the target range. In comparison, the production of the spectrum with the propagation done using the convected Helmholtz equation is a matter of minute but with major flaws in the prediction of the directivity. Moreover, this method allows the perspective of the prediction of the installation effects, which would not be possible with the simplified propagation, while remaining in the target range of restitution time.

VI. Conclusion

In this paper was presented a methodology to predict fine-scale jet mixing noise using both the source modelling described by Tam and Auriault and geometrical acoustics to account for the propagation. First, the theoretical framework from Tam and Auriault was presented before explaining how it could be reduced to a simpler problem using a propagation in two associated homogeneous media. Geometrical acoustics was used to form a complete prediction model. The model is assessed on the EXEJET configuration. The predictions presented here showed promising results, especially concerning on peak amplitude and the presence of the cone of silence. The method has proven to be quite accurate on a isolated jet while allowing results to be produced in less than an hour thus making it a powerful tool on an industrial point of view. Further tests should be done in order to complete the assessment of the model with the prediction of installation effects. This method should also be tested on a simpler nozzle associated with a cold jet to have the jet plume as closer as a homogeneous medium as possible.

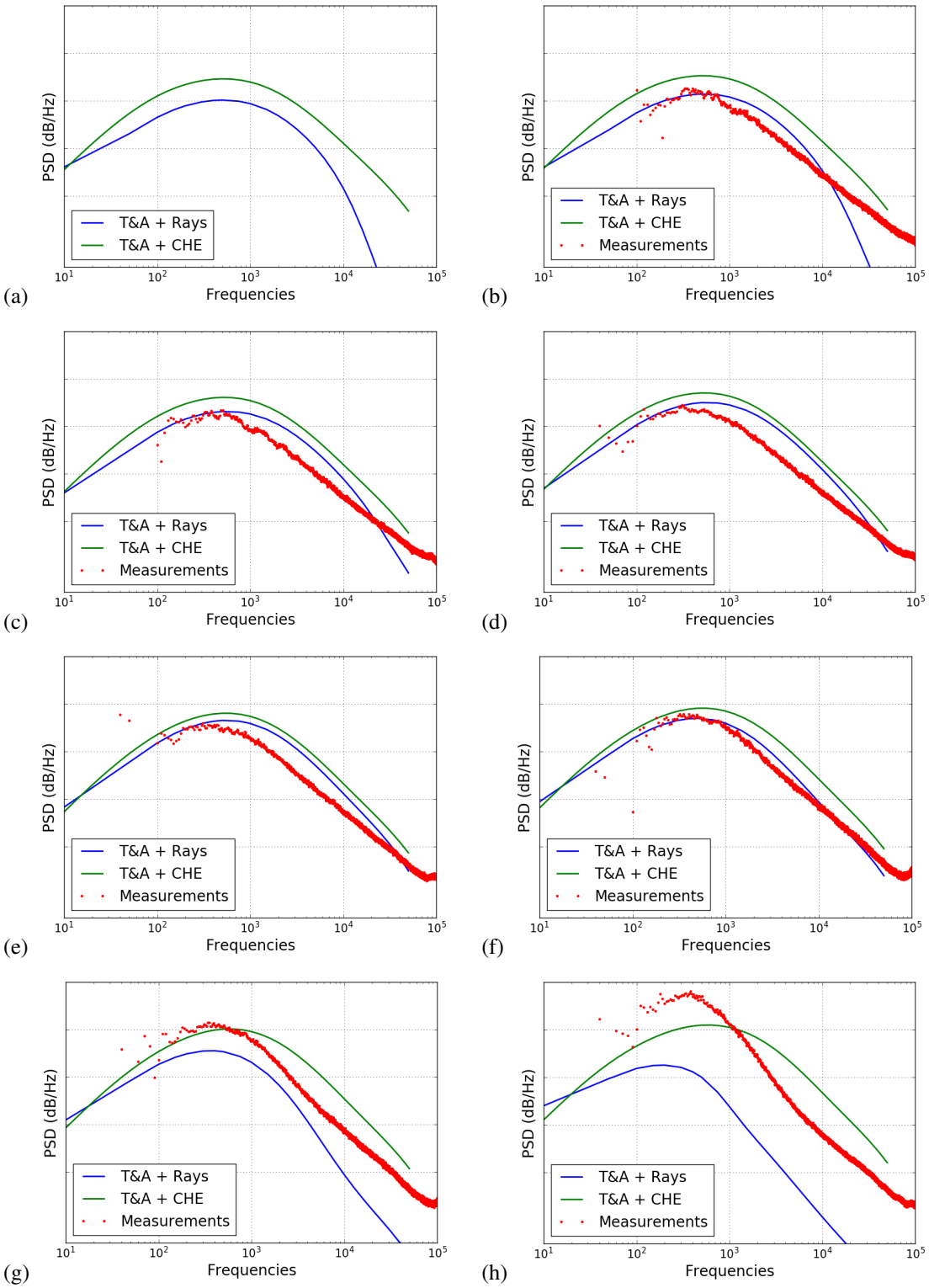

Fig. 5 PSD for both prediction models and measurements at a polar angle of (a) 45°, (b) 60°, (c) 75°, (d) 90°, (e) 105°, (f) 120°, (g) 135°, (h) 150°. The distance between two ticks is 10dB/Hz.

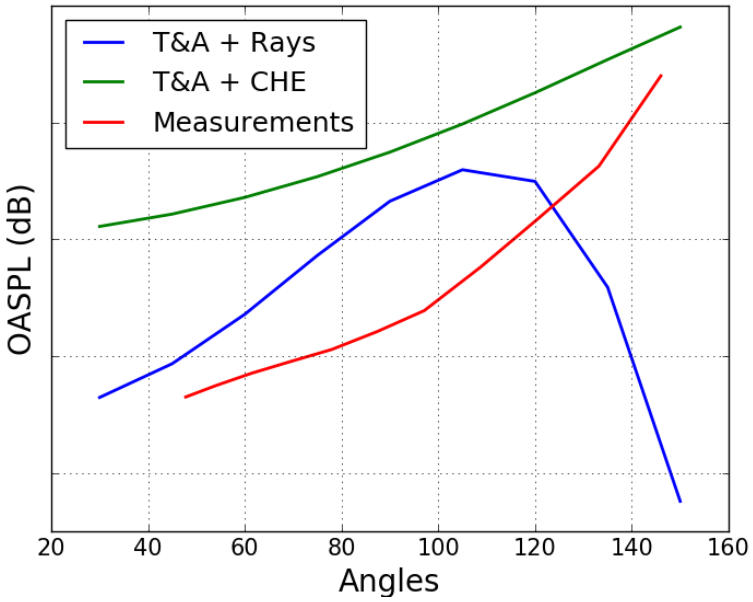

Fig. 6 OASPL for both prediction models and measurements. The distance between two ticks is 4dB.

Acknowledgments

This work was performed within the framework of the LABEX CeLyA (ANR-10-LABX- 0060) of Université de Lyon, within the program « Investissements d'Avenir » (ANR-16- IDEX-0005) operated by the French National Research Agency (ANR). It was also performed with the valuable help of Nolwenn Balin and Jérome Huber from Airbus.

A. Generalities about geometrical acoustics

A. Introduction of geometrical acoustics

The propagation of sound through the mixing layer or even through the whole jet is not straightforward. Each variation of speed or temperature in the surrounding medium will cause a local refraction that will bend the ray and thus completely change the propagation of the wave. The velocity and temperature gradients are in such a way that the ray travelling downstream will be deviated out of the jet creating a cone of silence [12]. Moreover, the presence of a foreign body in the propagation field will generates reflections and thus abrupt path changes.

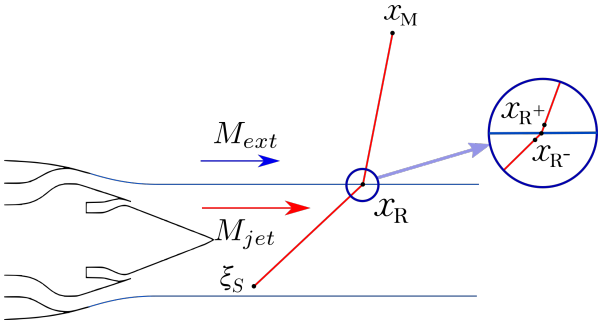

Fig. 7 Representation of a ray being refracted through the mixing layer

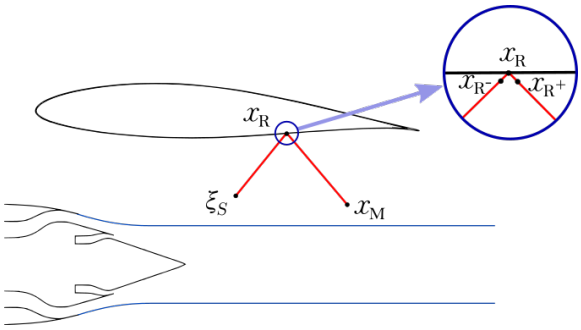

Fig. 8 Representation of a ray being reflected on a wing

This theory is explained in details, refer to Pathak et al [13] among others. For one ray going from $\vec{\xi}_S$ to $\vec{x}_M$ passing by $\vec{x}_R$ where a refraction or a reflection happens, as illustrated respectively in Fig. 7 and Fig. 8, the pressure in $\vec{x}_M$ is

$$\hat{G}(\vec{x}_M,\omega) = \hat{G}(\vec{x}_{R^-},\omega)K_D K_T \hat{\Phi}(\vec{x}_M,\vec{x}_{R^+},\omega) \tag{43}$$

where $\vec{x}_{R^-}$ is a point on the ray path right before the interface between the two media and thus before the refraction or reflection and $\vec{x}_{R^+}$ is a point on the ray path right after the interface between the two media and thus before the refraction or reflection.

$\hat{\Phi}$ is a phase shift expressed as

$$\hat{\Phi}(\vec{x}_M,\vec{x}_{R^+},\omega) = e^{ik'\left[|\vec{x'}_M - \vec{x'}_{R^+}| + M_{ext}(x'_M - x'_{R^+})\right]} \tag{44}$$

with M_{ext} the Mach number of the medium in which the second part of the ray is located and with this change of variable dependent on the Mach number of the medium in which the corresponding point is located

$$x = \sqrt{1 - M_{ext}^2}\,x' \tag{45}$$

$$y = y' \tag{46}$$

$$z = z' \tag{47}$$

$$k = \sqrt{1 - M_{ext}^2}\,k' \tag{48}$$

with $k = 2\pi/\lambda$ the wavenumber.

K_D is the divergence coefficient accounting for the loss of amplitude caused by the change of the curvature of the wavefront induced by the propagation of the wave. In a homogeneous medium it is readily seen that the classical attenuation in $1/r$ is found because the incident and emerging radii of curvature are identical. In the case of a curved interface between two media, these radii are not equal. The second one is the transmission factor K_T describing the change in amplitude upon switching propagation medium. Both factors are applied on the pressure. These two coefficients have to be introduced in order to properly take into account all the effects involved into the refraction phenomenon.

B. Reflection and refraction factor

By going through a change of medium and switching propagation indices, the ray will split in tow parts, a transmitted (or refracted) part and a reflected part. Both will be attenuated by a factor. The reflection factor K_R is given in [14] in the case of a ray going from a medium "jet" to a medium "ext". Here, ϕ_i is the angle between the incident ray and the normal to the surface and ϕ_e is the angle between the emerging ray en the normal to the surface.

$$K_R = \frac{\rho_{ext}c_{ext}^2\cos(2\phi_i) - \rho_{jet}c_{jet}^2\cos(2\phi_i)}{\rho_{ext}c_{ext}^2\cos(2\phi_i) + \rho_{jet}c_{jet}^2\cos(2\phi_e)} \tag{49}$$

and the refraction factor K_T, associated with the transmitted ray in the second medium, can be expressed as follows

$$K_T = \frac{2\rho_{ext}c_{ext}^2 \cos(2\phi_i)}{\rho_{ext}c_{ext}^2 \cos(2\phi_i) + \rho_{jet}c_{jet}^2 \cos(2\phi_e)} \tag{50}$$

with

$$K_T = 1 + K_R \tag{51}$$

C. The divergence coefficient

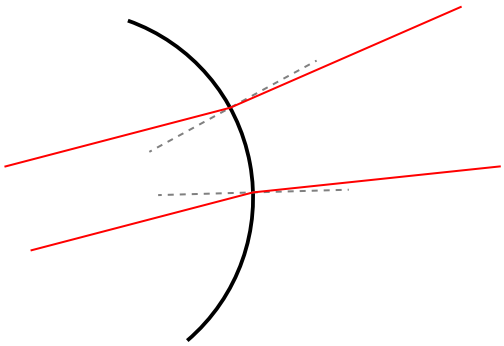

Fig. 9 Illustration of the divergence of a 2D ray induced by the passage through a curved interface with the normal to the surface shown in dotted line

A last effect has to be taken into account which is the fact that when passing through a curved interface or reflecting on a curved surface, the section of the pencil ray changes as pictured in Fig. 9. This is described by Deschamps [15]. The divergence coefficient is expressed that way

$$K_D = \sqrt{\frac{r_1^e r_2^e}{(r_1^e + s)(r_2^e + s)}} \tag{52}$$

with r^e being the radii of curvature of the emerging (or reflected) wave and with s the distance between the location of the refraction (or reflection) to the observer (or the next reflection/refraction). The calculation to obtain the radii of curvatures are detailed in [15] and will not be presented here for conciseness.

D. Formula for the pressure

For one ray, one can write the pressure as

$$\hat{p}'(\vec{x}_M, \omega) = I(\vec{\xi}_S, \omega)\hat{G}(\vec{x}_M, \vec{\xi}_S, \omega) \tag{53}$$

with I the amplitude of the source and $\hat{G}$ the propagation function from the source to the observer.

$\hat{G}$ can be obtained with either just the convected Helmholtz equation or the convected Helmholtz equation for the first segment completed with as many application of Eq. (43) as there is reflections or refractions. Once this is done for each ray, the pressure at the location of the observer is obtained with the summation of all the contribution of each ray.

E. Application of geometrical acoustics: Practical case

A realistic case will be taken in order to show the practical use of geometrical acoustics . Let's consider the situation pictured in Fig. 10 of three rays coming from two source points $\vec{\xi}_S$ and $\vec{\zeta}_S$ of respective amplitude $I(\vec{\xi}_S, \omega)$ and $I(\vec{\zeta}_S, \omega)$. One ray is going out of the jet, impacting the wing and going through the jet before reaching the observer $\vec{x}_M$ (path 1.2) while the others are simply exiting the jet and reaching $\vec{x}_M$ (path 1.1 and 2.1).

The pressure in $\vec{x}_M$ is expressed using Eq. (53) giving the following formula

$$\hat{p}'(\vec{x}_M,\omega) = I(\vec{\xi}_S,\omega)\left(\hat{G}_{1.1}(\vec{x}_M,\vec{\xi}_S,\omega) + \hat{G}_{1.2}(\vec{x}_M,\vec{\xi}_S,\omega)\right) + I(\vec{\zeta}_S,\omega)\hat{G}_{2.1}(\vec{x}_M,\vec{\zeta}_S,\omega) \tag{54}$$

with $\hat{G}_n$ the propagation term for each path. As an illustration, this term for the path 1.2 will be explicited.

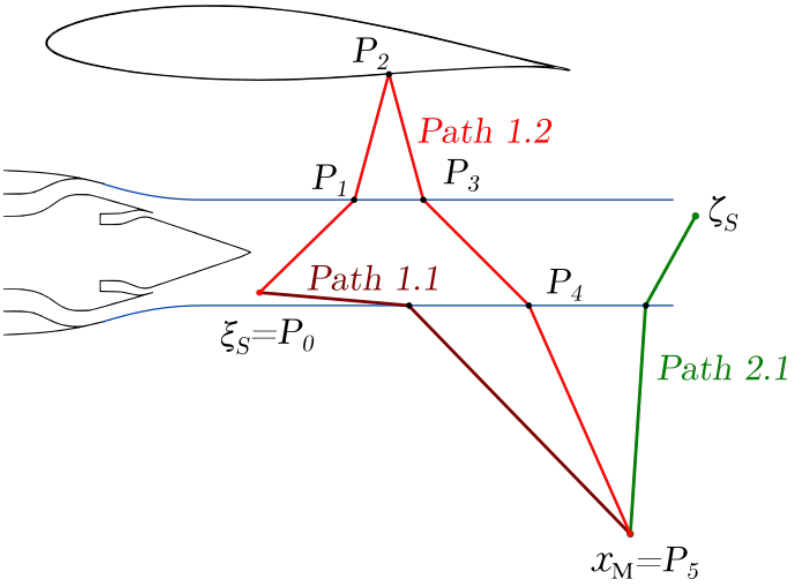

Fig. 10 Practical case of a ray with multiple refractions and reflections

Using Eq. (43) for each refraction or reflection, the propagation part for the the ray can be written. That makes for the contribution to the pressure in $\vec{x}_M$ by the ray 1.2

$$\hat{p}'_{1.2}(\vec{x}_M,\omega) = \hat{p}'(\vec{P}_4^-,\omega)\hat{K}(\vec{x}_M,\vec{P}_4,\omega) \tag{55}$$

$$\hat{p}'(\vec{P}_4^-,\omega) = \hat{p}'(\vec{P}_3^-,\omega)\hat{K}(\vec{P}_4,\vec{P}_3,\omega) \tag{56}$$

$$\hat{p}'(\vec{P}_3^-,\omega) = \hat{p}'(\vec{P}_2^-,\omega)\hat{K}(\vec{P}_3,\vec{P}_2,\omega) \tag{57}$$

$$\hat{p}'(\vec{P}_2^-,\omega) = \hat{p}'(\vec{P}_1^-,\omega)\hat{K}(\vec{P}_2,\vec{P}_1,\omega) \tag{58}$$

using the following notation for conciseness

$$\hat{K}(\vec{P}_{n+1},\vec{P}_n,\omega) = K_D(\vec{P}_n)K_T(\vec{P}_n)\hat{\Phi}(\vec{P}_{n+1}^-,\vec{P}_n^+,\omega) \tag{59}$$

where K_D and K_T are calculated with the correct formula whether it is a refraction or a reflection.

That leads to

$$\hat{p}'_{1.2}(\vec{x}_M,\omega) = \hat{p}'(\vec{P}_1^-,\omega)\prod_{n=1}^{4}\hat{K}(\vec{P}_{n+1},\vec{P}_n,\omega) \tag{60}$$

Finally, the last step is the propagation from $\vec{\xi}_S$ to $\vec{x}_{P_1^-}$, which is done with the convected Helmholtz equation. That gives, for a source amplitude in $\vec{\xi}_S$ noted $I(\vec{\xi}_S)$ and the solution to the equation noted $\hat{G}'(\vec{x}_S,\vec{x}_{P_1},\omega)$

$$\hat{p}'_{1.2}(\vec{x}_M,\omega) = I(\vec{\xi}_S)\hat{G}(\vec{\xi}_S,\vec{P}_1,\omega)\prod_{n=1}^{4}\hat{K}(\vec{P}_{n+1},\vec{P}_n,\omega) = I(\vec{\xi}_S)\hat{G}_{1.2}(\vec{x}_M,\vec{\xi}_S,\omega) \tag{61}$$

F. Formula in the general case

Now that a practical case has been presented, the formula in the general case can be deduced. Eq. (53) can be written in the general case of N sources as

$$\hat{p'}(\vec{x},\omega) = \sum_{n=1}^{N} I(\vec{\xi}_{S_n}) \sum_{r=1}^{N_n} \hat{G}_r(\vec{x},\vec{\xi}_{S_n},\omega) \tag{62}$$

where N_n is the number of rays starting from the source point $\vec{\xi}_{S_n}$ and reaching the observer $\vec{x}_M$.

By using a volume of sources and thus a volumic amplitude for each source it leads to the following integral formulation

$$\hat{p'}(\vec{x},\omega) = \int_{\vec{\xi}_S} I(\vec{\xi}_S) \sum_{r=1}^{N(\vec{\xi}_S)} \hat{G}_r(\vec{x},\vec{\xi}_S,\omega) d\vec{\xi}_S \tag{63}$$

with the transfer function $\hat{G}$ being

$$\hat{G}(\vec{\xi}_S,\vec{x},\omega) = \sum_{r=1}^{N(\vec{\xi}_S)} \hat{G}_r(\vec{x},\vec{\xi}_S,\omega) \tag{64}$$

In the time domain, that makes

$$p'(\vec{x},t) = \int_{\vec{\xi}_S} \int_{\omega} \int_{t_1} I(\vec{\xi}_S) \hat{G}(\vec{\xi}_S,\vec{x},\omega) e^{-i\omega(t-t_1)} d\vec{\xi}_S d\omega dt_1 \tag{65}$$

References

[1] Tam, C. K. W., and Auriault, L., "Jet Mixing Noise from Fine-Scale Turbulence," *AIAA Journal*, Vol. 37, No. 2, 1999, pp. 145–153.

[2] Morris, P., and Boluriaan, S., "The Prediction of Jet Noise from CFD Data," *10th AIAA/CEAS Aeroacoustics Conference*, Vol. 3, 2004.

[3] Miller, S. A. E., "Toward a comprehensive model of jet noise using an acoustic analogy," *AIAA Journal*, Vol. 52, No. 10, 2014, pp. 2143–2164.

[4] Tam, C. K. W., Golebiowski, M., and Seiner, J. M., "On the two components of turbulent mixing noise from supersonic jets," *AIAA Paper*, 1996-1716.

[5] Bogey, C., and Marsden, O., "Simulations of initially highly disturbed jets with experiment-like exit boundary layers," *AIAA Journal*, Vol. 54, No. 4, 2016, pp. 1299–1312.

[6] Huber, J., Drochon, G., Pintado-Peno, A., Cléro, F., and Bodard, G., "Large-Scale Jet Noise Testing, Reduction and Methods Validation "EXEJET": 1. Project Overview and Focus on Installation," *20th AIAA/CEAS Aeroacoustics Conference, Atlanta GA, USA*, 2014.

[7] Davies, P. O. A. L., Fisher, M. J., and Barratt, M. J., "The characteristics of the turbulence in the mixing region of a round jet," *Journal of Fluid Mechanics*, 1962, pp. 337–367.

[8] Tam, C. K. W., Viswanathan, K., Ahuja, K. K., and J., P., "The sources of jet noise: experimental evidence," *Journal of Fluid Mechanics*, Vol. 615, 2008, pp. 253–292.

[9] Brouwer, H. H., and Nijboer, R. J., "Computation of Fine-Scale Turbulence Jet Noise," *Internal NLR report*, 2005.

[10] Pierce, A. D., *Acoustics : an introduction to its physical principles and applications*, Acoustical Society of America, New York, 1989.

[11] Fleury, V., Bailly, C., Jondeau, E., Michard, M., and Juvé, D., "Space-Time Correlations in Two Subsonic Jets Using Dual Particle Image Velocimetry Measurements," *AIAA Journal*, Vol. 46, No. 10, 2008, pp. 2498–2509.

[12] Tam, C. K. W., and Auriault, L., "Mean flow refraction effects on sound radiated from localized sources in a jet," *Journal of Fluid Mechanics*, Vol. 370, 1998, pp. 149–174.

[13] Pathak, P., Burnside, W., and Marhefka, R., "A uniform GTD analysis of the diffraction of electromagnetic waves by a smooth convex surface," *IEEE Transactions on Antennas and Propagation*, Vol. 28, No. 5, 1980, pp. 631–642.

[14] Morse, P. M., and Ingard, K. U., *Theoretical Acoustics*, Princeton University Press, Princeton, New Jersey, 1968.

[15] Deschamps, G. A., "Ray techniques in electromagnetics," *Proc. IEEE*, Vol. 60, September 1972, pp. 1022 – 1035.